Optimal Allocation of Local Feedback in Multistage Amplifiers via Geometric Programming

Joel L. Dawson, Stephen P. Boyd, *Fellow, IEEE*, Maria del Mar Hershenson, and Thomas H. Lee

***Abstract*—We consider the problem of optimally allocating local feedback to the stages of a multistage amplifier. The local feedback gains affect many performance indexes for the overall amplifier, such as bandwidth, gain, rise time, delay, output signal swing, linearity, and noise performance, in a complicated and nonlinear fashion, making optimization of the feedback gains a challenging problem. In this paper, we show that this problem, though complicated and nonlinear, can be formulated as a special type of optimization problem called *geometric programming*. Geometric programs can be solved globally and efficiently using recently developed interior-point methods. Our method, therefore, gives a complete solution to the problem of optimally allocating local feedback gains, taking into account a wide variety of constraints.**

***Index Terms*—Amplifiers, analog circuits, circuit optimization, design automation, geometric programming, sensitivity.**

I. Introduction

THE USE of linear feedback around an amplifier stage was pioneered by Black [1], Bode [2], and others. The relation between the choice of feedback gain and the (closed-loop) gain, bandwidth, rise-time, sensitivity, noise, and distortion properties, is well understood (see, e.g., [3]). For a single-stage amplifier, the choice of the (single) feedback gain is a simple problem.

In this paper we consider the *multistage* amplifier shown in Fig. 1, consisting of n open-loop amplifier stages denoted $A_1, \ldots, A_n$, with local feedback gains $f_1, \ldots, f_n$ employed around the stages.

We assume that the amplifier stages are fixed, and consider the problem of choosing the feedback gains $f_1, \ldots, f_n$. The choice of these feedback gains affects a wide variety of performance measures for the overall amplifier, including gain, bandwidth, rise time, delay, noise, distortion, and sensitivity properties, maximum output swing, and dynamic range. These performance measures depend on the feedback gains in a complicated and nonlinear manner. It is thus far from clear, given a set of specifications, how to find an optimal choice of feedback gains. We refer to the problem of determining optimal values of the feedback gains, for a given set of specifications on overall amplifier performance, as the *local feedback allocation problem*.

We will show that the local feedback allocation problem can be cast as a *geometric program* (GP), which is a special type of optimization problem. Even complicated GPs can be solved very efficiently, and globally, by recently developed interior-point methods (see [4]–[6]). Therefore, we are able to give a complete, global, and efficient solution to the local feedback allocation problem.

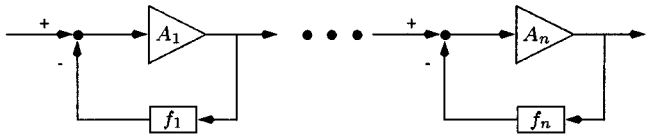

Fig. 1. Block diagram of multistage amplifier.

In Section II, we give a detailed description of the models of an amplifier stage used to analyze the performance of the amplifier. Though simple, the models capture the basic qualitative behavior of a source-degenerated differential pair. In Section III, we derive expressions for the various performance measures for the overall amplifier, in terms of the local feedback gains. In Section IV, we give a brief description of geometric programming, and in Section V, we put it all together to show how the optimal local feedback allocation problem can be cast as a GP. Design examples are given in Section VI, and analysis for a cascade of source-coupled pairs is performed in the Appendix.

II. Amplifier Stage Models

In this section we describe several different models of an amplifier stage, used for different types of analysis.

A. Linearized Static Model

The simplest model we use is the linear static model shown in Fig. 2. The stage is characterized by $y_i = \alpha_i e_i$, where α_i is the gain of the ith stage, which we assume to be positive. We will use this simple model for determining the overall gain of the amplifier, determining the maximum signal swing, and the sensitivity of the amplifier gain to each stage gain.

B. Static Nonlinear Model

To quantify nonlinear distortion effects, we will use a static nonlinear model of the amplifier stage as shown in Fig. 3. We assume that the nonlinearity or transfer characteristic has the form

$$y_i = a_i(e) = \alpha_i e - \beta_i e^3 + o(e^3). \tag{1}$$

This form is inspired by the transfer characteristic of a source-coupled pair [7], and is a general model for third-order nonlinearity in a stage with an odd transfer characteristic. The function $a_i(\cdot)$ is called the *transfer characteristic* of the ith stage, and β_i is called the *third-order coefficient* of the amplifier stage. Note

Manuscript received January 2, 2000; revised May 4, 2000. This paper was recommended by Associate Editor G. Palumbo.

The authors are with the Department of Electrical Engineering, Stanford University, Stanford, CA 94305-4070 USA (e-mail: jldawson@smirc.stanford.edu).

Publisher Item Identifier S 1057-7122(01)00649-3.

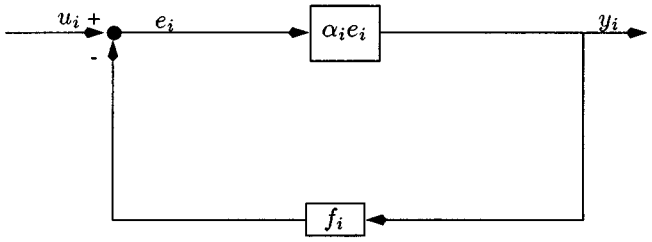

Fig. 2. Linearized static model of amplifier stage.

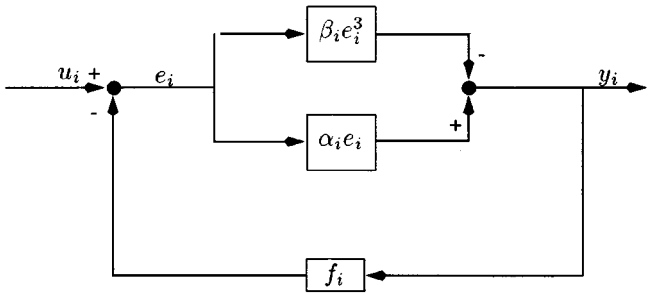

Fig. 3. Nonlinear static model of amplifier stage.

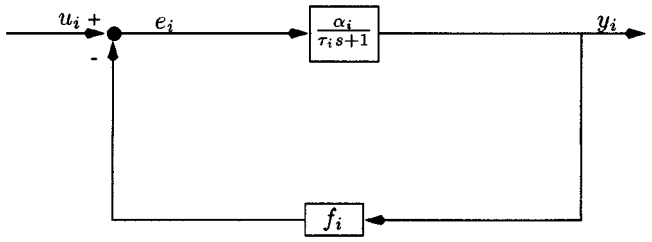

Fig. 4. Linear dynamic model of amplifier stage.

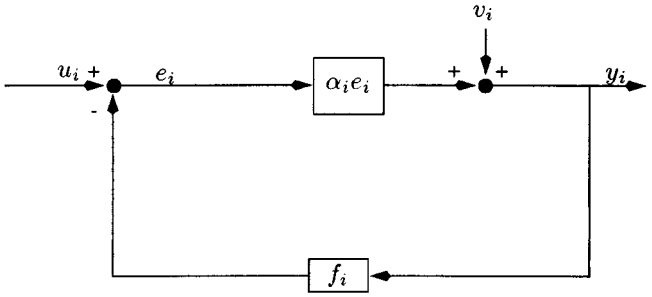

Fig. 5. Static noise model of amplifier stage.

that the gain and third-order coefficient are related to the transfer characteristic by

$$\alpha_i = a_i'(0) \qquad \beta_i = -\frac{a_i'''(0)}{6}. \tag{2}$$

We assume that $\beta_i \geq 0$, which means the third-order term is *compressive*: as the signal level increases from zero, the nonlinear term tends to decrease the output amplitude when compared to the linear model.

C. Linearized Dynamic Model

To characterize the bandwidth, delay, and rise time of the overall amplifier, we use the linearized dynamic model shown in Fig. 4. Here the stage is represented by a simple one-pole transfer function with time constant τ_i (which we assume to be positive).

D. Static Noise Model

Finally, we have the static noise model shown in Fig. 5, which includes a simple output-referred noise v_i. As will become clear later, more complicated noise models including input noise, or noise injected in the feedback loop, are also readily handled by our method. Our noise model is characterized by the rms value of the noise source, which we denote $\overline{v_i}$. We assume that noise sources associated with different stages are uncorrelated.

III. Amplifier Analysis

In this section, we derive expressions for various performance indexes for the overall amplifier, which we express in terms of the *return differences* of the stages, defined as

$$l_i = 1 + f_i \alpha_i. \tag{3}$$

A. Gain and Output Swing

We consider the linear static model of Section II-A. The gain of the amplifier, from input u_1 to the output of the kth stage y_k, is given by

$$\prod_{i=1}^{k} \frac{\alpha_i}{1+\alpha_i f_i} = \prod_{i=1}^{k} \frac{\alpha_i}{l_i} \tag{4}$$

and the overall gain, from u_1 to y_n, is given by

$$\tilde{\alpha} = \prod_{i=1}^{n} \frac{\alpha_i}{l_i}. \tag{5}$$

Here, of course, α_i/l_i is the familiar expression for the closed-loop gain of the ith stage. It will be convenient later to use the notation

$$\tilde{\alpha}_i = \frac{\alpha_i}{l_i} \tag{6}$$

to denote the closed-loop gain of the ith stage. (In general, we will use the tilde to denote a closed-loop expression.)

Now suppose the input signal level is $U = |u_1|$, and that the ith stage has a maximum allowed output signal level of Y_i, i.e., we require $|y_i| \leq Y_i$. This in turn means that for $k = 1, \ldots, n$, we have

$$U \prod_{i=1}^{k} \frac{\alpha_i}{l_i} \leq Y_k \tag{7}$$

so the maximum allowed input signal level is

$$U_{\max} = \max_{k=1,\ldots,n} Y_k \prod_{i=1}^{k} \frac{l_i}{\alpha_i}. \tag{8}$$

The maximum allowed output signal level is found by multiplying by the overall gain

$$Y_{\max} = \max_{k=1,\ldots,n} Y_k \prod_{i=k+1}^{n} \frac{\alpha_i}{l_i} \tag{9}$$

(where the empty product, when $i = n$, is interpreted as one).

B. Sensitivity

The (logarithmic) sensitivity of the overall amplifier gain to the open-loop gain of the ith stage is given by

$$S_i = \frac{\partial \log \tilde{\alpha}}{\partial \log \alpha_i} = \frac{1}{l_i}. \tag{10}$$

C. Nonlinearity

We begin by deriving the closed-loop third-order coefficient of a single feedback amplifier stage, using the static nonlinear model of Section II-B. The output y is related to the input u through the relation

$$y = a(u - fy). \tag{11}$$

Differentiating both sides with respect to u leads to the familiar result from elementary feedback theory

$$y'(0) = \frac{a'(0)}{1 + fa'(0)} = \frac{\alpha}{l} = \tilde{\alpha}. \tag{12}$$

Differentiating again yields

$$y''(0) = \frac{a''(0)}{l^3} = 0 \tag{13}$$

and, once more

$$y'''(0) = \frac{a'''(0)l - 3fa''(0)^2}{l^5} = -\frac{6\beta}{l^4} \tag{14}$$

using $a'''(0) = -6\beta$ and $a''(0) = 0$ from the previous equation. This equation shows that the third-order coefficient of the closed-loop transfer characteristic is given by

$$\tilde{\beta} = \frac{y'''(0)}{6} = \frac{\beta}{l^4}. \tag{15}$$

This is the well-known result showing the linearizing effect of (linear) feedback on an amplifier stage.

Next, let us consider a cascade of two amplifier stages. Let the transfer characteristics of two stages be $y_1(\cdot)$ and $y_2(\cdot)$. We write

$$\phi_2(u) = y_2(y_1(u)) \tag{16}$$

and differentiate

$$\begin{aligned} \phi_2'(0) &= y_2'(0)y_1'(0) \\ \phi_2''(0) &= y_2'(0)y_1''(0) + (y_1'(0))^2 y_2''(0) \end{aligned} \tag{17}$$

and so

$$\begin{aligned} \phi_2'''(0) = {} & y_2'(0)y_1'''(0) + y_1'(0)^3 y_2'''(0) \\ & + 3y_2''(0)y_1'(0)y_1''(0). \end{aligned} \tag{18}$$

Since y_1 and y_2 are both odd functions, the last term vanishes. This shows that the third-order coefficient of the cascade of the two stages in given by

$$\tilde{\beta}_1 \tilde{\alpha}_2 + \tilde{\beta}_2 \tilde{\alpha}_1^3. \tag{19}$$

More generally, the third-order coefficient of a cascade of n stages can be expressed as

$$\tilde{\beta} = \sum_{i=1}^{n} \left[\left(\prod_{k=1}^{i-1} \tilde{\alpha}_k^3 \right) \tilde{\beta}_i \left(\prod_{j=i+1}^{n} \tilde{\alpha}_j \right) \right]. \tag{20}$$

This very complicated formula gives the relation between the local return differences and the third-order coefficient of the overall amplifier.

D. Bandwidth

We next examine the linearized dynamic performance of the amplifier chain, using the stage model given in Section II-C. The transfer function of an individual stage is given by

$$\frac{Y_i(s)}{U_i(s)} = \frac{\alpha_i/(\tau_i s + 1)}{1 + f_i \alpha_i/(\tau_i s + 1)} = \frac{\tilde{\alpha}_i}{\tilde{\tau}_i s + 1} \tag{21}$$

where $\tilde{\tau}_i = \tau_i / l_i$ is the closed-loop time constant of the ith stage. The transfer function of the entire cascade amplifier immediately follows

$$H(s) = \prod_{i=1}^{n} \frac{\tilde{\alpha}_i}{\tilde{\tau}_i s + 1}. \tag{22}$$

The -3-dB bandwidth of the amplifier is defined as the smallest frequency ω for which $|H(j\omega)| = |H(0)|/\sqrt{2}$.

E. Delay and Rise Time

The rise time and delay of the overall amplifier can be characterized in terms of the moments of the impulse response, as described in [8]. The delay is the normalized first moment of the impulse response of the system

$$t_d = \frac{\int_{-\infty}^{\infty} t h(t)\, dt}{\int_{-\infty}^{\infty} h(t)\, dt}. \tag{23}$$

Using basic properties of the Laplace transform and results from Section III-D, we have

$$\begin{aligned} t_d &= \frac{-\left.\dfrac{dH(s)}{ds}\right|_{s=0}}{H(0)} = -\left.\frac{d}{ds} \prod_{i=1}^{n} \frac{1}{\tilde{\tau}_i s + 1}\right|_{s=0} \\ &= \sum_{i=1}^{n} \tilde{\tau}_i = \sum_{i=1}^{n} \frac{\tau_i}{l_i}. \end{aligned} \tag{24}$$

This formula shows the exact relation between the overall amplifier delay (as characterized by the first moment of the impulse response) and the local return differences l_i.

We use the second moment of the impulse response,

$$t_r^2 = 4 \left[\frac{\int_{-\infty}^{\infty} t^2 h(t)\, dt}{\int_{-\infty}^{\infty} h(t)\, dt} - t_d^2 \right] \tag{25}$$

as a measure of the square of the rise time of the overall amplifier in response to a step input. Again, making use of Laplace trans-

form identities, we express (25) in terms of the transfer function $H(s)$

$$t_r^2 = \frac{4}{H(0)}\left[\frac{d^2}{ds^2}H(s)\bigg|_{s=0} - t_d^2\right]. \tag{26}$$

Substituting the transfer function of the amplifier, given in (22), we find that the rise time of the overall amplifier is

$$t_r^2 = 4\sum_{i=1}^{n}\frac{\tau_i^2}{l_i^2} \tag{27}$$

(using the fact that the closed-loop rise time of the ith stage is $2\tilde{\tau}_i$).

F. Noise and Dynamic Range

We now consider the static noise model of Section II-D. The mean-squared noise amplitude at the output of the overall amplifier can be written

$$\overline{v_{\text{out}}^2} = \sum_{i=1}^{n}\left(\frac{\overline{v_i^2}}{l_i^2}\left[\prod_{j=i+1}^{n}\frac{\alpha_j}{l_j}\right]^2\right). \tag{28}$$

The input-referred mean-squared noise is then

$$\overline{v_{\text{in}}^2} = \frac{\overline{v_{\text{out}}^2}}{\tilde{\alpha}^2} = \sum_{i=1}^{n}\left(\frac{\overline{v_i^2}}{\alpha_i^2}\left[\prod_{j=1}^{i-1}\frac{l_j}{\alpha_j}\right]^2\right). \tag{29}$$

The *dynamic range* (DR) of the amplifier is the ratio of maximum output range to output referred rms noise level, expressed in decibels

$$\text{DR} = 20\log_{10}\frac{Y_{\max}}{\sqrt{\overline{v_{\text{out}}}}}. \tag{30}$$

G. SFDR and IIP Linearity Measures

We conclude this analysis by obtaining expressions for the spurious-free dynamic range (SFDR) and the input-referred third-order intercept point (IIP3). They are both readily derived from the results in Section III-C–III-F, and so contain no new information or analysis, but they are widely used performance indices for the amplifier.

SFDR and IIP3 give information about the linearity of an amplifier. They concern the results of the following experiment: inject a signal $v\cos\omega_1 t + v\cos\omega_2 t$ at the input, and examine the output for the presence of intermodulation (IM) products. We concern ourselves here with third-order IM products, which owe their existence to nonzero β_i. The third-order intermodulation products are

$$\left[\frac{3}{4}\tilde{\beta}v^3\right][\cos(\omega_1+2\omega_2)t + \cos(\omega_1-2\omega_2)t + \cos(2\omega_1+\omega_2)t + \cos(2\omega_1-\omega_2)t]. \tag{31}$$

The SFDR is defined as the signal-to-noise ratio when the power in each third-order IM product equals the noise power at the output [9]. It is straightforward to derive: simply refer a third-order IM product back to the input and equate to the input-referred rms noise amplitude

$$\frac{1}{\tilde{\alpha}}\left[\frac{3}{4}\tilde{\beta}v^3\right] = \sqrt{\overline{v_{\text{in}}}}. \tag{32}$$

The SFDR in decibels is then given by

$$\text{SFDR} = \frac{2}{3}(10)\log_{10}\left(\frac{\frac{4}{3}\left|\frac{\tilde{\alpha}}{\tilde{\beta}}\right|}{\overline{v_{\text{in}}^2}}\right). \tag{33}$$

The IIP3 is the input power at which the amplitude of the third-order IM products equals the input. Mathematically, we require

$$|\tilde{\alpha}v| = \left|\frac{4}{3}\tilde{\beta}v^3\right|. \tag{34}$$

Normalizing the input resistance to unity for convenience, we have for IIP3

$$\text{IIP} = \frac{2}{3}\left|\frac{\tilde{\alpha}}{\tilde{\beta}}\right|. \tag{35}$$

IV. Geometric Programming

Let f be a real-valued function of n real, positive variables $x_1, x_2, \ldots, x_n$. It is called a *posynomial* function if it has the form

$$f(x_1,\ldots,x_n) = \sum_{k=1}^{t} c_k x_1^{\alpha_{1k}} x_2^{\alpha_{2k}} \ldots x_n^{\alpha_{nk}} \tag{36}$$

where $c_j \geq 0$ and $\alpha_{ij} \in \boldsymbol{R}$. When $t = 1$, f is called a *monomial* function. Thus, for example, $0.7 + 2x_1/x_3^2 + x_2^{0.3}$ is posynomial and $2.3(x_1/x_2)^{1.5}$ is a monomial. Posynomials are closed under sums, products, and nonnegative scaling.

A *geometric program* (GP) has the form

$$\begin{aligned} \text{minimize} \quad & f_0(x) \\ \text{subject to} \quad & f_i(x) \leq 1, \qquad i = 1,2,\ldots,m \\ & g_i(x) = 1, \qquad i = 1,2,\ldots,p \\ & x_i > 0, \qquad i = 1,2,\ldots,n \end{aligned} \tag{37}$$

where f_i are posynomial functions and g_i are monomial functions. GPs were introduced by Duffin, Peterson, and Zener in the 1960s [10].

The most important property of GPs for us is that they can be solved, with great efficiency, and globally, using recently developed interior-point methods [6], [4]. Geometric programming has recently been used to optimally design electronic circuits including CMOS op-amps [11], [12], and planar spiral inductors [13].

Several simple extensions are readily handled by geometric programming. If f is a posynomial and g is a monomial, then the constraint $f(x) \leq g(x)$ can be expressed as $f(x)/g(x) \leq 1$ (since f/g is posynomial). In particular, constraints of the form $f(x) \leq a$, where $a > 0$ is a constant, can also be used. Similarly, if g_1 and g_2 are both monomial functions, the constraint $g_1(x) = g_2(x)$ can be expressed as $g_1(x)/g_2(x) = 1$ (since g_1/g_2 is monomial). If g is a monomial, we can maximize it by minimizing the posynomial function $1/g$.

A. Geometric Programming in Convex Form

A GP can be reformulated as a *convex optimization problem*, i.e., the problem of minimizing a convex function subject to

convex inequalities constraints and linear equality constraints. This is the key to our ability to globally and efficiently solve GPs. We define new variables $y_i = \log x_i$, and take the logarithm of a posynomial f to get

$$h(y) = \log(f(e^{y_1}, \ldots, e^{y_n})) = \log\left(\sum_k^t e^{a_k^T y + b_k}\right) \quad (38)$$

where $a_k^T = [\alpha_{1k} \ \cdots \ \alpha_{nk}]$ and $b_k = \log c_k$. It can be shown that h is a *convex* function of the new variable y: for all $y, z \in \boldsymbol{R}^n$ and $0 \leq \lambda \leq 1$ we have

$$h(\lambda y + (1-\lambda)z) \leq \lambda h(y) + (1-\lambda)h(z). \quad (39)$$

Note that if the posynomial f is a monomial, then the transformed function h is affine, i.e., a linear function plus a constant.

We can convert the standard GP (37) into a convex program by expressing it as

$$\begin{array}{ll} \text{minimize} & \log f_0(e^{y_1}, \ldots, e^{y_n}) \\ \text{subject to} & \log f_i(e^{y_1}, \ldots, e^{y_n}) \leq 0, \qquad i = 1, \ldots, m \\ & \log g_i(e^{y_1}, \ldots, e^{y_n}) = 0, \qquad i = 1, \ldots, p. \end{array} \quad (40)$$

This is the so-called *convex form* of the GP (37). Convexity of the convex form GP has several important implications: we can use efficient interior-point methods to solve them, and there is a complete and useful duality, or sensitivity theory for them [4].

B. Solving Geometric Programs

Since Ecker's survey paper there have been several important developments related to solving GPs in the exponential form. A huge improvement in computational efficiency was achieved in 1994, when Nesterov and Nemirovsky developed efficient interior-point algorithms to solve a variety of nonlinear optimization problems, including geometric programs [6]. Recently, Kortanek *et al*. have shown how the most sophisticated primal–dual interior-point methods used in linear programming can be extended to geometric programming, resulting in an algorithm approaching the efficiency of current interior-point linear programming solvers [14]. The algorithm they describe has the desirable feature of exploiting sparsity in the problem, i.e., efficiently handling problems in which each variable appears in only a few constraints.

For our purposes, the most important feature of GPs is that they can be *globally* solved with great efficiency. Problems with hundreds of variables and thousands of constraints are readily handled, on a small workstation, in minutes; the problems we encounter in this paper, which have a few tens of variables and fewer than 100 constraints, are easily solved in under 1 s.

Perhaps even more important than the great efficiency is the fact that algorithms for geometric programming always obtain the global minimum. Infeasibility is unambiguously detected: if the problem is infeasible, then the algorithm will determine this fact, and not just fail to find a feasible point. Another benefit of the global solution is that the initial starting point is irrelevant: the same global solution is found no matter what the initial starting point is.

These properties should be compared to general methods for nonlinear optimization, such as sequential quadratic programming, which only find *locally* optimal solutions, and cannot unambiguously determine infeasibility. As a result, the starting point for the optimization algorithm does have an effect on the final point found. Indeed, the simplest way to lower the risk of finding a local, instead of global, optimal solution, is to run the algorithm several times from different starting points. This heuristic only reduces the risk of finding a nonglobal solution. For geometric programming, in contrast, the risk is always exactly zero, since the global solution is always found regardless of the starting point.

V. Optimal Local Feedback Allocation

We now make the following observation, based on the results of Section III: a wide variety of specifications for the performance indexes of the overall amplifier can be expressed in a form compatible with geometric programming using the variables l_i. The startling implication is that optimal feedback allocation can be determined using geometric programming.

The true optimization variables are the feedback gains f_i, but we will use instead the return differences l_i, with the constraints $l_i \geq 1$ imposed to ensure that $f_i \geq 0$. Once we determine the optimal values for l_i, we can find the optimal feedback gains via

$$f_i = (l_i - 1)/\alpha_i. \quad (41)$$

A. Closed-Loop Gain

The closed-loop gain $\tilde{\alpha}$ is given by the monomial expression (5). Therefore, we can impose any type of constraint on the closed-loop gain: we can require it to equal a given value, or specify a minimum or maximum value for the closed-loop gain. Each of these constraints can be handled by geometric programming.

B. Maximum Signal Swing

The maximum output signal swing is given by (9). The constraint that the output swing exceed a minimum required value, i.e., $Y_{\max} \geq \gamma$, can be expressed as

$$Y_k \prod_{i=k+1}^{n} \frac{\alpha_i}{l_i} \geq \gamma, \qquad k = 1, \ldots, n. \quad (42)$$

Each of these inequalities is a monomial inequality, and hence can be handled by geometric programming. Note that we also allow the bound on signal swing, i.e., γ, as a variable here.

C. Sensitivity

The sensitivity of the amplifier to the ith stage gain is given by the monomial expression (10). It follows that we can place an upper bound on the sensitivity (or, if we choose, a lower bound or equality constraint).

D. Bandwidth

Consider the constraint that the closed-loop -3 dB bandwidth should exceed Ω. Since the magnitude of the transfer function of the amplifier is monotonically decreasing as a function of frequency, this is equivalent to imposing the constraint

$$|H(j\Omega)| \geq \frac{1}{\sqrt{2}} H(0) \quad (43)$$

which we can rewrite as

$$\frac{1}{|H(j\Omega)|^2} \leq \frac{2}{H(0)^2}. \tag{44}$$

Now using the expression for the transfer function

$$H(j\omega) = \prod_{i=1}^{n} \frac{\alpha_i}{j\tau_i\omega + l_i} \tag{45}$$

we can write the bandwidth constraint as

$$\left|\frac{1}{H(j\Omega)}\right|^2 = \prod_{i=1}^{n} \frac{(\tau_i\Omega)^2 + l_i^2}{\alpha_i^2} \leq 2\prod_{i=1}^{n} \frac{l_i^2}{\alpha_i^2}. \tag{46}$$

In turn, we can express this as

$$\prod_{i=1}^{n} \frac{(\tau_i\Omega)^2 + l_i^2}{l_i^2} \leq 2. \tag{47}$$

This is a complicated, but posynomial, inequality in the variables l_i, hence it can be handled by geometric programming. Note that we can even make the minimum -3 dB bandwidth Ω a variable, and maximize it.

E. Noise and Dynamic Range

Expression (29) for the input-referred noise power, is a posynomial function of the variables $l_1, \ldots, l_n$. Therefore, we can impose a maximum on the input-referred noise level, using geometric programming.

The requirement that the dynamic range exceed some minimum allowed value $\mathrm{DR}_{\min}$, i.e., $\mathrm{DR} \geq \mathrm{DR}_{\min}$, can be expressed as

$$\frac{\overline{v_{\mathrm{out}}^2}}{\gamma} \leq 10^{-\mathrm{DR}/10} \tag{48}$$

where γ is the bound on signal swing defined in (42). Therefore, this constraint can be handled by geometric programming.

F. Delay and Rise Time

As can be seen in (24) and (27), the expressions for delay and rise time are posynomial functions of the return differences l_i. A maximum on each can thus be imposed.

G. Third-Order Distortion

The expression for third-order coefficient, given in (20), is a posynomial, so we can impose a maximum on the third-order coefficient.

H. SFDR and IIP3

Consider the constraint that the SFDR should exceed some minimum value γ. Using the expression (33), we can write this as

$$\frac{2}{3}(10)\log_{10}\left(\frac{\frac{4}{3}\left|\frac{\tilde{\alpha}}{\tilde{\beta}}\right|}{\overline{v_{\mathrm{in}}^2}}\right) \geq \gamma. \tag{49}$$

This can be written as

$$\frac{4}{3}\frac{\tilde{\alpha}}{\tilde{\beta}}\frac{1}{\overline{v_{\mathrm{in}}^2}} \geq 10^{3\gamma/20}. \tag{50}$$

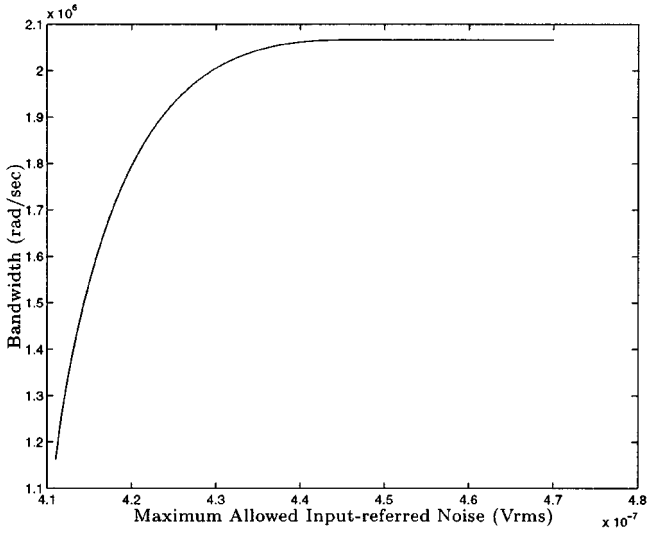

Fig. 6. Maximum bandwidth versus limit on input-referred noise.

This can be handled by geometric programming by writing it as

$$\frac{\tilde{\beta}}{\tilde{\alpha}}\overline{v_{\mathrm{in}}^2} \leq \frac{3}{4}10^{-3\gamma/20}. \tag{51}$$

VI. Design Examples

We have shown that complicated problems of feedback allocation can be solved, globally and efficiently, using geometric programming. We can take as an objective any of the posynomial performance measures described above, and apply any combination of the constraints described above. We can also compute optimal tradeoff curves by varying one of the specifications or constraints over a range, computing the optimal value of the objective for each value of the specification.

We provide in this section a few system-level examples. In the Appendix, we demonstrate a circuit-level application using the common source-coupled pair.

A. Tradeoffs Among Bandwidth, Gain, and Noise

In our first example we consider a three-stage amplifier, with all stages identical, with parameters

$$\alpha_i = 10 \qquad \tau_i = 10^{-6}\ \mathrm{s} \qquad \overline{v_{n,i}} = 4.07\ \mu\mathrm{V}. \tag{52}$$

The required closed-loop gain is 23.5 dB. We maximized the bandwidth, subject to the equality constraint on closed-loop gain, and a maximum allowed value of input-referred noise.

Fig. 6 shows the optimal bandwidth achieved, as a function of the maximum allowed input-referred noise. As it must, the optimal bandwidth increases as we relax (increase) the input-referred noise limit. Fig. 7 shows the optimal values of the feedback gains as the input-referred noise limit varies.

These curves roughly identify two regions in the design space. In one, the noise constraint is so relaxed as to not be an issue. The program identifies the optimum bandwidth solution for the given gain, which is to place all of the closed loop poles in the same place. In the other, the tradeoff between bandwidth and noise is strong. Equation (29) shows that the noise contribution of $\overline{v_{n,1}}$ is independent of l_1, but the noise contributions of the following stages can be diminished by

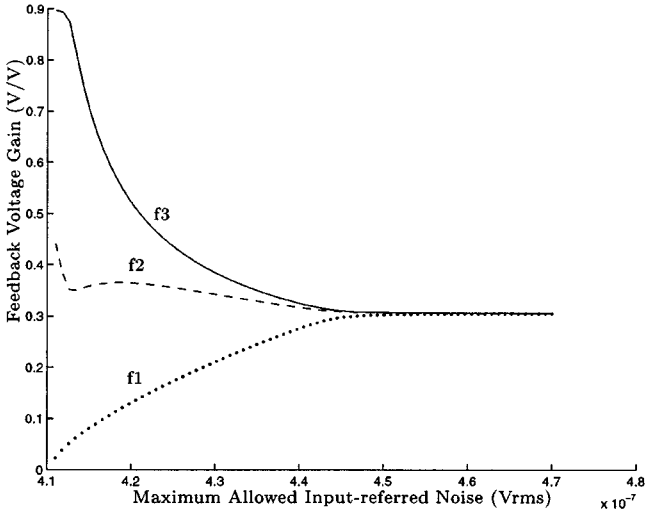

Fig. 7. Optimal feedback allocation pattern, for maximum bandwidth with limit on input-referred noise. Gain = 23.5 dB.

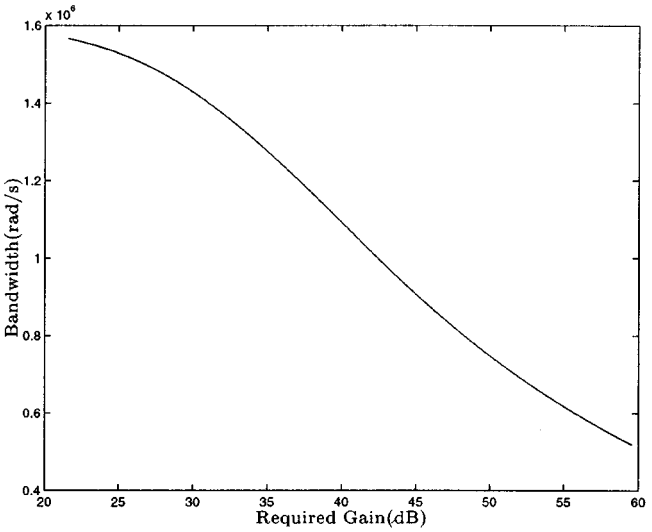

Fig. 8. Maximum bandwidth versus required closed-loop gain. Maximum input-referred noise = 4.15^{-7} V rms.

making l_1 (and therefore f_1) small. It follows that f_3 is the greatest of the feedback gains, followed by f_2 and f_1.

We can also examine the optimal tradeoff between bandwidth and required dc gain. Here we impose the fixed limit on input-referred noise at 4.14^{-7} V rms, and maximize the bandwidth subject to a required closed-loop gain.

Figs. 8 and 9 show the maximum attainable bandwidth and the optimal feedback gain allocation as a function of the required closed-loop gain. Again, we see two regions in design space caused by the noise constraint.

B. SFDR versus Gain

In this example, we again consider a three-stage amplifier, now with identical stages having parameters

$$\alpha_i = 10 \qquad \beta_i = 0.667\ \mathrm{V}^{-2} \qquad \overline{v_{n,i}} = 4.07\ \mu\mathrm{V}. \tag{53}$$

We maximize the spurious-free dynamic range subject to an equality constraint on the overall gain. Fig. 10 shows the

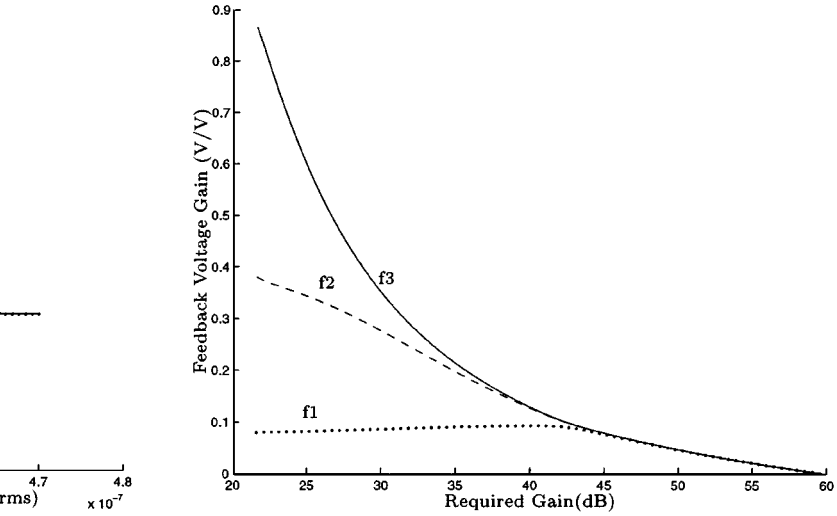

Fig. 9. Optimal feedback allocation pattern for maximum bandwidth versus required closed-loop gain. Maximum input-referred noise = 4.15^{-7} V rms.

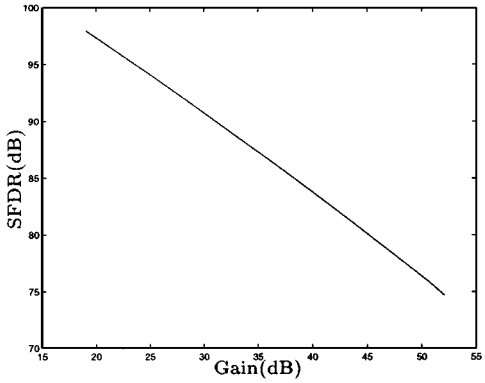

Fig. 10. Maximum spurious-free dynamic range versus required gain.

achieved SFDR as a function of the required gain, and Fig. 11 shows the associated optimal gain allocation patterns.

In addition to obtaining optimal designs from the Figs. 10 and 11, we observe a qualitative trend: feedback gain is allocated preferentially to stages furthest down the signal chain. This is in agreement with sound engineering judgment, and with the results of Section VI-A.

We can also argue from the standpoint of optimum linearity that Fig. 11 makes sense. Nonlinearity in the later stages, where the signal amplitude is the largest, will cause the most severe harmonic distortion. It follows that feedback should be applied more aggressively in later stages.

C. Stage Selection

The method described in this paper computes the globally optimal values of the local feedback gains, with the amplifier models fixed. We can use the method indirectly to optimally choose each stage, from a set of possible choices, in addition to optimally allocating feedback around the stages. Suppose we have a set of m possible choices for each of n stages. By computing the optimal performance for each m^n possible combinations of stages, we can then determine the optimal combination as well as the optimal feedback gains. Of course, the effort required to exhaustively search over the combinations grows

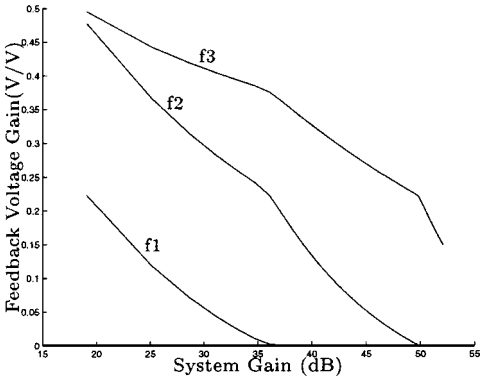

Fig. 11. Optimal feedback allocation pattern for maximum spurious-free dynamic range versus required gain.

TABLE I
CANDIDATE STAGES

Amplifier Designation	α_i	β_i	$\overline{v_n}$
A	10	0.67	$41\mu V$
B	10	6.7	$4.1\mu V$
C	10	67	$0.41\mu V$

rapidly with the number of stages, but is certainly feasible for moderate numbers of stages, e.g., fewer than six or so.

We demonstrate this method for optimal stage selection with an example. Table I shows a listing of three candidate stages for use in a multistage amplifier design. Amplifier A can be seen to have best linearity and the worst noise; amplifier C has the worst linearity and the best noise, and amplifier B is in between.

Our goal is to maximize SFDR, subject to a required gain of 46 dB, for a three-stage design. By solving all 27 combinations, we find that the optimal combination of stages and feedback is

Stage 1: amplifier C, with $f = 0.00023$.
Stage 2: amplifier B, with $f = 0.06589$.
Stage 3: amplifier A, with $f = 0.20072$,

which achieves the optimal SFDR of 85 dB.

This solution makes sense: the low-noise stage is used for the first stage (which is more critical for noise, since its noise is amplified by subsequent stages); the high-linearity stage is used for the last stage (which handles larger signals, and so is more critical for distortion). Note that in this particular case, the optimal solution is to operate the first two stages essentially open loop.

VII. CONCLUSION

We have shown how to globally and efficiently solve the problem of optimally allocating local feedback gains in a multistage amplifier by posing the problem in the form of a GP. This formulation can handle a wide variety of practical objectives and constraints, and allows us to rapidly compute globally optimal tradeoff curves between competing specifications.

We mention several extensions which are readily handled. It is not hard to work out the corresponding (posynomial) formulas for distortion characteristics that are not symmetric, in which the second-order term dominates. It is also easy to handle a more sophisticated noise model, in which the noise is injected at several locations in the feedback around each stage, and not just at the output as in the current model. In each case, the resulting noise power expression is still posynomial, and, therefore, can be handled by geometric programming. Another extension is to couple the design of the feedback together with the actual component-level design of the amplifier (for example, transistor widths and lengths) as in [15].

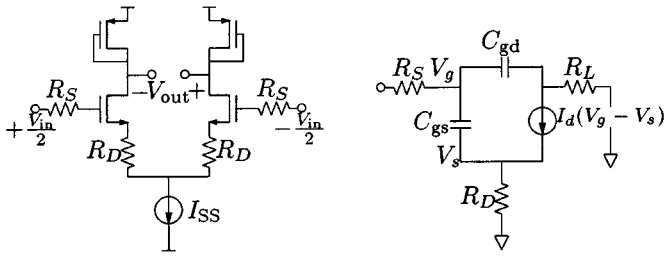

Fig. 12. CMOS source-coupled pair and differential half-circuit.

We envision several situations where the methods described in this paper would be very useful to a circuit designer. Whenever the number of stages is at least three, and the number of important specifications is at least three (say), the problem of optimally allocating local feedback gains becomes quite complex, and a tool that completely automates this process is quite useful. When the number of stages reaches five or six, and the absolute optimal performance is sought, our method will far outperform even a good designer adjusting gains in an *ad hoc* manner.

APPENDIX
AN APPLICATION

The foregoing analysis has established feedback allocation as a solvable problem. The extension of our technique to real-world applications, however, begs clarification: we have (seemingly) ignored loading between stages, chosen suspiciously simple single-pole dynamics, etc. We thus include this appendix, in which we consider the ubiquitous source-coupled pair as our basic open-loop stage. Local feedback is allocated in the form of source degeneration, and all other characteristics (bias currents, load resistances, transistor sizes, etc.) are fixed.[1]

Fig. 12 shows the basic stage that we consider. The differential half-circuit on the right should not be taken to represent the traditional "small-signal" model, as the dependent current source models a MOSFET operating in the saturation regime. The capacitors $C_{\rm gs}$ and $C_{\rm gd}$ *are* linear capacitors [9], and the PMOS devices provide the resistances R_L. We show in the sequel how this common structure maps to the theoretical framework outlined in Section II.

A. Linearized Static Model

For this model, the capacitors shown in Fig. 12 become open circuits, and the mapping from Figs. 2 to 13 is straightforward. A few short lines of algebra lead to the familiar gain expression

$$A_v = \left(\frac{g_m}{1 + g_m R_D}\right) R_L. \tag{54}$$

Already, it can be seen that l_i from the foregoing analysis finds its place here as $(1+g_m R_D)_i$, with R_D taking the place of feedback gain. We emphasize that this is not merely a mathematical

[1]These, too, can be optimized via geometric programming; see [12] and [11].

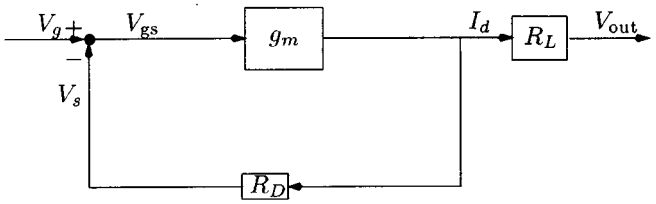

Fig. 13. Source degeneration as a form of feedback.

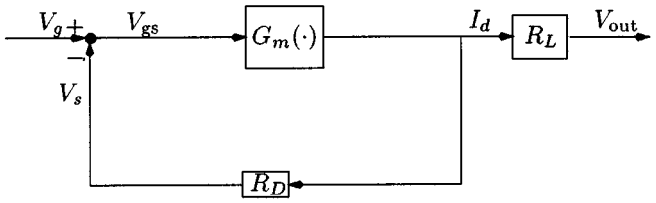

Fig. 14. Modification for nonlinear static model.

accident, but points to the physically meaningful interpretation of degeneration as a feedback mechanism.

B. Static Nonlinear Model

In Fig. 14, we modify Fig. 13 by replacing g_m with $G_m(\cdot)$, the nonlinear expression for drain current as a function of $V_{\rm gs}$. The expression for differential output current as a function of differential input voltage for a source-coupled pair is given in Gray and Meyer [7]. We reproduce it here, where I_d and V_i are understood to be differential signals

$$I_d = \mu_n \frac{C_{\rm ox} W}{2L} V_i \sqrt{\left(\frac{2I_{\rm SS}}{\mu_n \left(\frac{C_{\rm ox} W}{2L} \right)} \right) - (V_i)^2}. \tag{55}$$

All constants in this formula are MOSFET parameters, and $I_{\rm SS}$ is the value of the current source in Fig. 12. A Taylor expansion of the square root allows us to write $G_m(\cdot)$ as

$$G_m(V_{\rm gs}) = \alpha V_{\rm gs} - \beta V_{\rm gs}^3 + \gamma V_{\rm gs}^5 - \cdots. \tag{56}$$

This is consistent with Fig. 3.

C. Linearized Dynamic Model

We use the Miller approximation described in Gray and Meyer [7], modified here to account for source degeneration. The Miller approximation (see Fig. 15) is the recognition that the dynamics of a single stage are dominated by a single pole, which arises from the interaction between source resistance R_S and the input capacitance. With no source degeneration, this input capacitance would be the sum of $C_{\rm gs}$ and the Miller multiplied $C_{\rm gd}$

$$C_T = C_{\rm gs} + (1 + g_m R_L) C_{\rm gd} \simeq C_{\rm gs} + (g_m R_L) C_{\rm gd} \tag{57}$$

where we have made the approximation that the gain $A_v = g_m R_L$ is significantly greater than unity. This capacitance, together with the source resistance, creates a pole with time constant τ

$$\tau = R_S (C_{\rm gs} + (g_m R_L) C_{\rm gd}). \tag{58}$$

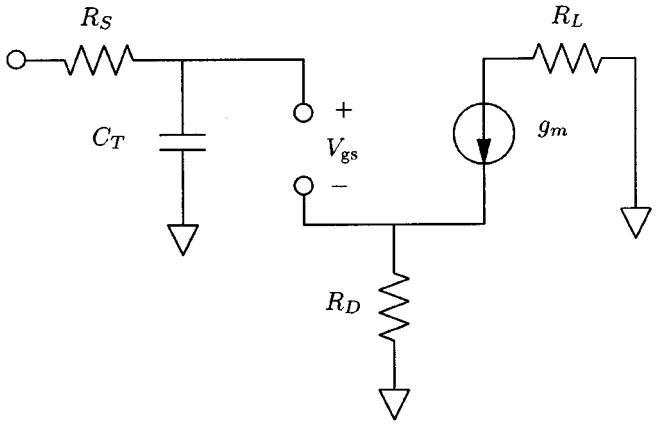

Fig. 15. Modeling dynamics using the Miller approximation.

Source degeneration causes the real part of the impedance looking into the gate to increase. At frequencies below the transistor's f_T, however, the capacitive part still dominates and we replace $C_{\rm gs}$ in the Miller formulation with

$$\frac{C_{\rm gs}}{1 + g_m R_D}. \tag{59}$$

Source degeneration reduces the gain of the stage from $g_m R_L$ to

$$\tilde{A}_v = \frac{g_m R_L}{1 + g_m R_D}. \tag{60}$$

Our C_T capacitance is accordingly modified to

$$\tilde{C_T} \simeq \frac{C_{\rm gs}}{1 + g_m R_D} + \left(\frac{g_m R_L}{1 + g_m R_D} \right) C_{\rm gd}. \tag{61}$$

(We continue to assume that $\tilde{A}_v$ is much greater than unity.) Finally, it can be seen that the effect of feedback has been to reduce the time constant of the pole by a factor of the return difference $1 + g_m R_D$, exactly as was shown in Section III-D

$$\tilde{\tau} = R_S \tilde{C_T} = \frac{\tau}{1 + g_m R_D}. \tag{62}$$

If we define τ as in (58), it can be seen that the source-coupled pair maps perfectly to Fig. 4.

Finally, note that the dynamics here, which are the poles formed by the output impedance of stage i with the input capacitance of stage $i+1$, *are* the interstage loading effects.

1) An Alternative Formulation: Open-Circuit Time Constants: For bandwidth optimization in pure circuit systems, it is often useful to use the method of open-circuit time constants. The method may be summarized as computing the resistance R_i seen across the terminals of capacitors C_i with all other capacitors considered open circuits. The frequency $\omega = (1/\sum_i R_i C_i)$ has been shown to be a good estimate of the -3 dB bandwidth for many common circuits. Moreover, this estimate, when applicable, is always conservative. We direct the interested reader to the excellent discussions in [7] and [9].

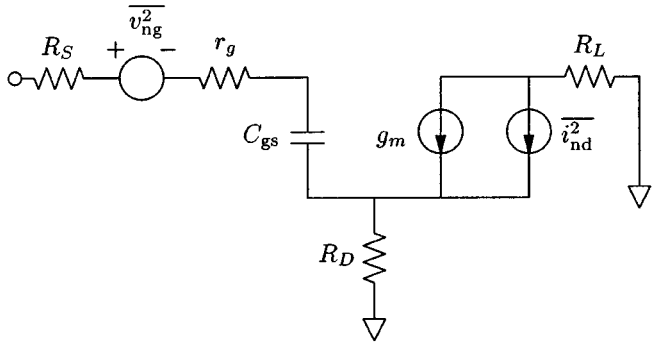

Fig. 16. MOSFET noise model.

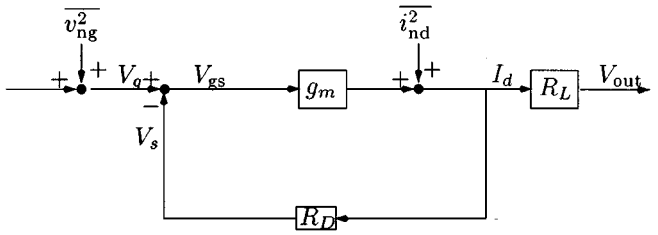

Fig. 17. MOSFET gate and drain noise.

We present this method as an alternative. For a given stage, the open-circuit resistance for $C_{\rm gd}$ can be shown to be

$$R_{\rm gd} = R_S + R_L + \frac{g_m}{1+g_m R_D} R_S R_L \tag{63}$$

a simple posynomial in the design variable $l = 1 + g_m R_D$. For $C_{\rm gs}$, the result is

$$R_{\rm gs} = \frac{R_S + R_D}{1+g_m R_D} \tag{64}$$

which we write as the posynomial in l

$$R_{\rm gs} = \frac{1}{g_m} + \left(R_S - \frac{1}{g_m}\right) l^{-1}. \tag{65}$$

D. Static Noise Model

There are two sources of noise in MOSFETs with a common physical origin: drain noise and gate noise [9]. Fig. 16 shows their places in the MOSFET model. Their corresponding places in our theoretical framework are clear, and shown in Fig. 17. We have only shown the noise sources associated with the active device itself. Resistors are known to introduce noise as well, and their contribution is straightforward to include. The noise of R_L, for example, is naturally incorporated as part of the gate noise of the following stage. Similar manipulations can be done for R_D and, of course, R_S.

E. Conclusion

In this Appendix we have shown how optimum local allocation of feedback can be applied to a common amplifier structure. Though we avoid explicit inclusion of loading effects in the main text, it can be seen that they can be included without disturbing the established framework.

References

[1] H. S. Black, "Stabilized feedback amplifiers," *Bell Syst. Tech. J.*, vol. 13, pp. 1–18, 1934.

[2] H. W. Bode, *Network Analysis and Feedback Amplifier Design*. New York: Van Nostrand, 1945.

[3] J. K. Roberge, *Operational Amplifiers: Theory and Practice*. New York: Wiley, 1975.

[4] S. Boyd and L. Vandenberghe. (1997) Introduction to convex optimization with engineering applications. Information Systems Laboratory, Stanford University. [Online]. Available: http://www.stanford.edu/class/ee364/

[5] J. Ecker, "Geometric programming: Methods, computations and applications," *SIAM Rev.*, vol. 22, no. 3, pp. 338–362, 1980.

[6] Y. Nesterov and A. Nemirovsky, *Interior-Point Polynomial Methods in Convex Programming*. Philadelphia, PA: SIAM, 1994, vol. 13, Studies in Applied Mathematics.

[7] P. R. Gray and R. G. Meyer, *Analysis and Design of Analog Integrated Circuits*. New York: Wiley, 1993.

[8] W. M. Siebert, *Circuits, Signals, and Systems*. Cambridge, MA: MIT Press, 1993.

[9] T. H. Lee, *The Design of CMOS Radio-Frequency Integrated Circuits*. New York: Cambridge Univ. Press, 1998.

[10] R. J. Duffin, E. L. Peterson, and C. Zener, *Geometric Programming—Theory and Applications*. New York: Wiley, 1967.

[11] M. Hershenson, S. Boyd, and T. H. Lee, "GPCAD: A tool for CMOS op-amp synthesis," in *IEEE/ACM Int. Conf. Computer Aided Design*, San Jose, CA, 1998, pp. 296–303.

[12] ——, "Automated design of folded-cascode op-amps with sensitivity analysis," in *Int. Conf. Electronics, Circuits and Systems*, vol. 1, Sept. 1998, p. 1.

[13] M. Hershenson, S. Mohan, S. Boyd, and T. H. Lee, "Optimization of inductor circuits via geometric programming," in *36th Design Automation Conf.*, 1999, pp. 994–998.

[14] K. O. Kortanek, X. Xu, and Y. Ye, "An infeasible interior-point algorithm for solving primal and dual geometric progams," *Mathematical Programming*, vol. 76, no. 1, pp. 155–181, 1997.

[15] M. Hershenson, S. Boyd, and T. H. Lee, "Optimal design of a CMOS op-amp via geometric programming," in *Applied and Computational Control, Signals, and Circuits*, B. Datta, Ed. Cambridge, MA: Birkhauser, 2000, vol. 2.

Joel L. Dawson received the S.B. and M.Eng. degrees in electrical engineering from the Massachusetts Institute of Technology, Cambridge, MA, in 1996 and 1997, respectively.

He is currently pursuing the Ph.D. degree in the Department of Electrical Engineering at Stanford University, Stanford, CA, and his research focus is on linearization techniques for RF power amplifiers.

Mr. Dawson has received the Stanford Graduate Fellowship, a National Science Foundation fellowship, and a Bell Laboratories CRFP fellowship. He was a Hertz Foundation finalist, and holds one U.S. patent.

Stephen P. Boyd (S'82–M'85–SM'97–F'99) received the A.B. degree in mathematics from Harvard University, Cambridge, MA, in 1980 and the Ph.D. degree in electrical engineering and computer science from the University of California, Berkeley, in 1985.

In 1985, he joined the Electrical Engineering Department at Stanford University, Stanford, CA, where he is now a Professor and Director of the Information Systems Laboratory. His interests include computer-aided control system design and convex programming applications in control, signal processing, and circuits.

Maria del Mar Hershenson was born in Barcelona, Spain. She received the B.S.E.E. degree from the Universidad Pontificia de Comillas, Madrid, Spain, in 1995 and the M.S. and Ph.D. degrees in electrical engineering from Stanford University, Stanford, CA, in 1997 and 1999, respectively.

In 1994, she was an intern at Linear Technology Corporation, Milpitas, CA, where she worked on low-power voltage regulators. Since the summer of 1999, she has been with Barcelona Design, Inc., Mountain View, CA, where she designs analog circuits. Her research interests are RF power amplifiers and convex optimization techniques applied to the automated design of analog integrated circuits.

Dr. Hershenson received an IBM fellowship in 1998.

Thomas H. Lee received the S.B., S.M. and Sc.D. degrees in electrical engineering, all from the Massachusetts Institute of Technology, Cambridge, MA, in 1983, 1985, and 1990, respectively.

He joined Analog Devices in 1990 where he was primarily engaged in the design of high-speed clock recovery devices. In 1992, he joined Rambus Inc., Mountain View, CA where he developed high-speed analog circuitry for 500 Mbyte/s CMOS DRAM's. He has also contributed to the development of PLL's in the StrongARM, Alpha and K6/K7 microprocessors. Since 1994, he has been an Assistant Professor of Electrical Engineering at Stanford University, Stanford, CA, where his research focus has been on gigahertz-speed wireline and wireless integrated circuits built in conventional silicon technologies, particularly CMOS. He holds twelve U.S. patents and is the author of a textbook, *The Design of CMOS Radio-Frequency Integrated Circuits* (Cambridge, MA: Cambridge Press, 1998) and is a coauthor of two additional books on RF circuit design. He is also a cofounder of Matrix Semiconductor.

Dr. Lee has twice received the "Best Paper" award at the International Solid-State Circuits Conference, was co-author of a "Best Student Paper" at ISSCC, and recently won a Packard Foundation Fellowship. He is a Distinguished Lecturer of the IEEE Solid-State Circuits Society, and was recently named a Distinguished Microwave Lecturer.